

Topological Graph Neural Networks

Max Horn^{1, 2, *} Edward De Brouwer^{3, *} Michael Moor^{1, 2} Yves Moreau³
 Bastian Rieck^{1, 2, *, †}, and Karsten Borgwardt^{1, 2, †}

¹Department of Biosystems Science and Engineering, ETH Zurich, 4058 Basel, Switzerland

²SIB Swiss Institute of Bioinformatics, Switzerland

³ESAT-STADIUS, KU LEUVEN, 3001 Leuven, Belgium

*These authors contributed equally.

†These authors jointly supervised this work.

Abstract

Graph neural networks (GNNs) are a powerful architecture for tackling graph learning tasks, yet have been shown to be oblivious to eminent substructures, such as cycles. We present TOGL, a novel layer that incorporates global topological information of a graph using persistent homology. TOGL can be easily integrated into *any type* of GNN and is strictly more expressive in terms of the Weisfeiler–Lehman test of isomorphism. Augmenting GNNs with our layer leads to beneficial predictive performance, both on synthetic data sets, which can be trivially classified by humans but not by ordinary GNNs, and on real-world data.

1. Introduction

Graphs are a natural description of structured data sets in many domains, including bioinformatics, image processing, and social network analysis. Numerous methods address graph learning problems such as graph classification or node classification. *Graph neural networks* (GNNs) describe a flexible set of architectures for graph learning tasks and have seen many successful applications over recent years. At their core, many GNNs are based on iterative message passing schemes. Since these schemes are collating information over the neighbours of every node, GNNs cannot necessarily capture certain simple topological structures in graphs, such as cycles.

By contrast, methods based on topological features, commonly summarised under the umbrella term of *topological data analysis* (TDA), have shown promising results in machine learning tasks. Focusing on coarse structures—such as the presence or absence of cycles—they can be used to provide multi-scale representations that capture the shape of complex structured and unstructured data sets. In this paper, we propose a Topological Graph Layer (TOGL) that can be easily integrated into any GNN to make it ‘topology-aware’. We thus obtain a generic way to augment existing GNNs and increase their expressivity in graph learning tasks.

Our contributions. We describe a layer based on TDA concepts that can be integrated into any GNN. Our layer is differentiable and capable of learning different topological representations of a graph. We prove that even by itself, our layer is strictly more expressive than any GNN since it incorporates the ability to work with multi-scale topological information in a graph. Moreover, we show that TOGL can improve predictive performance of a GNN when topological information is relevant for the task.

sentations of a graph. We prove that even by itself, our layer is strictly more expressive than any GNN since it incorporates the ability to work with multi-scale topological information in a graph. Moreover, we show that TOGL can improve predictive performance of a GNN when topological information is relevant for the task.

2. Background: Computational Topology

This paper considers undirected graphs, i.e. of the form $G = (V, E)$ with a set of vertices V and a set of edges $E \subseteq V \times V$. A simple set of topological features of G is given by their number of connected components β_0 and their number of cycles β_1 . These counts are also known as the *Betti numbers* in dimension 0 and dimension 1, respectively, and can be computed efficiently (we will discuss this below). Betti numbers are invariant under graph isomorphism; this is a consequence of a more general theorem in algebraic topology that incorporates higher-dimensional topological features as well (Hatcher, 2002, pp. 103–133). Thus, given two graphs G and G' with $G \simeq G'$, their Betti numbers will coincide. As with many invariants that are computationally efficient to compute, the converse relation does not hold, limiting their ability to discriminate between graphs. This is exacerbated by the fact that Betti numbers constitute mere feature counts. It is possible to increase their expressivity by assuming the existence of a *graph filtration*, i.e. a sequence of nested subgraphs of G such that

$$\emptyset = G^{(0)} \subseteq G^{(1)} \subseteq G^{(2)} \subseteq \cdots \subseteq G^{(n-1)} \subseteq G^{(n)} = G. \quad (1)$$

A filtration makes it possible to obtain more insights into the graph by ‘monitoring’ topological features of *each* $G^{(i)}$ and calculating their topological relevance, which is referred to as their *persistence*. If a topological feature appears for the first time in $G^{(i)}$ and disappears in $G^{(j)}$, we assign this feature a persistence of $j - i$. Equivalently, we can represent each of these features as a tuple (i, j) , which we collect in a *persistence diagram* \mathcal{D} . If a feature never disappears, we represent it by a tuple (i, ∞) ; such features are the ones that are counted for the respective Betti numbers. This process was formalised and extended to a wider class of structured data sets, namely simplicial complexes, and is known under the name of *persistent*

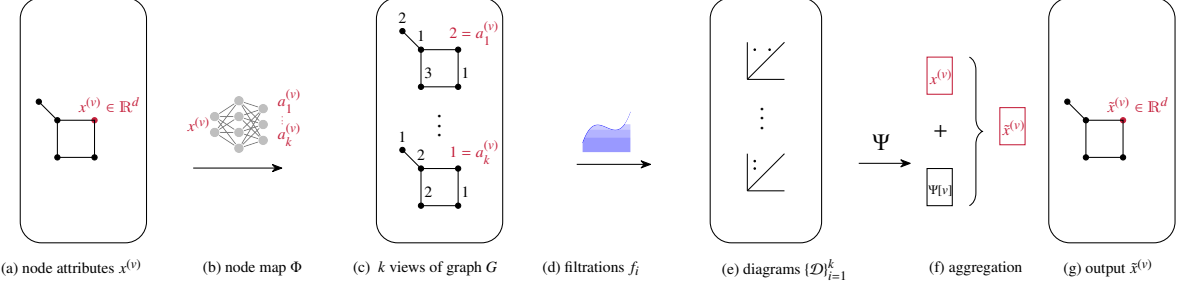
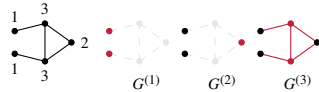


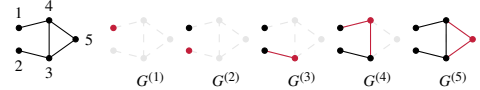
Figure 1.: Overview of TOGL, a topological graph layer. a) The node attributes $x^{(v)} \in \mathbb{R}^d$ of graph G serve as input. b) A network Φ_k maps $x^{(v)}$ to k node values $\{a_i^{(v)}\}_{i=1}^k$. c) Applying Φ_k to the attributes of each vertex v results in k views of graph G d) A vertex filtration f_i is computed for the i th view of G . e) Persistence diagrams $\{\mathcal{D}_i\}_{i=1}^k$ are encoded via the embedding function Ψ , where $\Psi[v]$ denotes the embedding of vertex v . f) The embedded topological features are combined with the input attributes $x^{(v)}$. g) Finally, this yields $\tilde{x}^{(v)} \in \mathbb{R}^d$ which acts as a new node representation augmented with multi-scale topological information.

homology, which has shown excellent promise in different areas of machine learning research (Carrière et al., 2020; Hofer et al., 2020; Kim et al., 2021; Moor et al., 2020; Rieck et al., 2019). We denote the calculation of persistence diagrams of a graph G under some filtration f by $\text{ph}(G, f)$. Typically, this will result in two persistence diagrams $\mathcal{D}_0, \mathcal{D}_1$, containing information about topological features in dimension 0 (connected components) and dimension 1 (cycles). Please refer to a Appendix B for a more technical description of persistent homology.

Filtrations are most conveniently thought of as arising from a function $f: G \rightarrow \mathbb{R}$, which assigns a scalar-valued function value to each node and edge of the graph by means of setting $f(u, v) := \max\{f(u), f(v)\}$ for an edge (u, v) . In this context, f is often picked to measure certain salient vertex features of G , such as the degree (Hofer et al., 2017), or its structural role in terms of a heat kernel (Carrière et al., 2020). The resulting topological features are then assigned the respective function values, i.e. $(i, j) \mapsto (f(u_i), f(u_j))$. As a brief example, consider a degree-based filtration of a simple graph. The filtration values are shown as numbers next to a vertex; we use $a^{(j)}$ to denote the filtration value at step j (this notation will be useful later when dealing with multiple filtrations). In each filtration step, the new nodes and edges added to the graph are shown in red, while black elements indicate the structure of the graph that already exists at this step.



Since all edges are inserted at $a^{(3)} = 3$, we obtain the following 0-dimensional persistence diagram $\mathcal{D}_0 = \{(1, \infty), (1, 3), (2, 3), (3, 3), (3, 3)\}$. The existence of a single tuple of the form (\cdot, ∞) indicates that $\beta_0 = 1$. Similarly, there is only one cycle in the data set, which is created at $a^{(3)}$, leading to $\mathcal{D}_1 = \{(3, \infty)\}$ and $\beta_1 = 1$. If we change the filtration such that each vertex has a *unique* filtration value, we obtain a different ordering and different persistence tuples, as well as more filtration steps:



Here, connected components are not all created ‘at once’, but more gradually, leading to $\mathcal{D}_0 = \{(1, \infty), (3, 3), (2, 4), (4, 4), (5, 5)\}$. Of particular interest is the tuple $(2, 4)$. It was created by the vertex with filtration value 2. In $G^{(3)}$ it merges with another connected component, namely the one created by the vertex with function value 3. This leads to the tuple $(3, 3)$, because in each merge, we merge from the ‘younger’ component (the one arising *later* in the filtration) to the ‘older’ component (the arising *earlier* in the filtration). Again, there is only a single cycle in the data set, which we detect at $a^{(5)} = 5$, leading to $\mathcal{D}_1 = \{(5, \infty)\}$.

Importantly, the cardinality of \mathcal{D}_0 is equal to the number of nodes n in the graphs and each tuple in the 0-dimensional diagram can be associated with the *vertex* that created it. As for \mathcal{D}_1 , its cardinality is the number of cycles. However, from a computational perspective, we pair each tuple in \mathcal{D}_1 with the *edge* that created it. Unpaired edges—edges that are not used to create a cycle—are given a dummy tuple value, such as $(0, 0)$. All other edges will be paired with the maximum value of the filtration, following previous work by Hofer et al. (2017).

As this example demonstrates, the expressive power of persistent homology is determined by the filtration. While we always obtain the right Betti numbers at the end of the filtration, the tuples that we observe during the filtration can make a large difference in understanding the structure of a graph. This suggests *learning* a proper filtration, a task that was addressed in previous work (Hofer et al., 2020), which also demonstrated that a learnt filtration improves predictive performance for classification approaches that only rely on topological information. We expand on this work by presenting a layer that can be easily integrated into *any* type of GNN, thus making it possible to create a true hybrid model that is provably more expressive than a GNN on its own.

3. TOGL: A Topological Graph Layer

We propose a new type of graph neural network layer that is capable of leveraging multi-scale topological information of input graphs. Subsequently, we give a brief overview of the components of this layer before discussing algorithmic details, theoretical expressivity, computational complexity, and limitations. An overview of the method is presented in Figure 1. For the sake of notational simplicity, we only assume that a single graph is being encoded, while in practice, the layer operates on *batches* of graphs.

The layer takes as input a graph $G = (V, E)$ equipped with a set of n vertices V and a set of edges E , along with a set of d -dimensional node attribute vectors $x^{(v)} \in \mathbb{R}^d$ for $v \in V$. These node attributes can either be node features of a data set or hidden representations learnt by some GNN. We employ a family of k vertex filtration functions of the form $f_i: \mathbb{R}^d \rightarrow \mathbb{R}$ for $i = 1, \dots, k$. Each filtration function f_i can focus on different properties of the graph. The image of f_i is finite and results in a set of node values $a_i^{(1)} < \dots < a_i^{(n)}$ such that the graph G is filtered according to $\emptyset = G_i^{(0)} \subseteq G_i^{(1)} \subseteq \dots \subseteq G_i^{(n)} = G$, where $G_i^{(j)} = (V_i^{(j)}, E_i^{(j)})$ and

$$\begin{aligned} V^{(i,j)} &:= \{v \in V \mid f_i(x^{(v)}) \leq a_i^{(j)}\} \\ E^{(i,j)} &:= \{v, w \in E \mid \max\{f_i(x^{(v)}), f_i(x^{(w)})\} \leq a_i^{(j)}\}. \end{aligned} \quad (2)$$

Given this filtration, we calculate a set of persistence diagrams, i.e. $\mathbf{ph}(G, f_i) = \{\mathcal{D}_i^{(0)}, \dots, \mathcal{D}_i^{(l)}\}$. Unless mentioned otherwise, $l = 1$, meaning that we are capturing connected components and cycles, but our implementation is not technically restricted to this; in general, higher values of l further increase the expressive power, while also increasing computational complexity (see Appendix A for a detailed discussion). Since the resulting persistence diagrams are cumbersome to work with, because they constitute sets of tuples in \mathbb{R}^2 , we use an *embedding function* $\Psi^{(l)}: \{\mathcal{D}_1^{(l)}, \dots, \mathcal{D}_k^{(l)}\} \rightarrow \mathbb{R}^{n' \times d}$ for embedding persistence diagrams into a high-dimensional space that will be used to obtain the vertex representations, where n' is the number of *vertices* n if $l = 0$ and the number of *edges* if $l = 1$. This step is crucial as it enables us to use the resulting topological features as node features, making TOGL a layer that can be integrated into arbitrary GNNs. We later explain the precise mapping of $\Psi^{(l)}$ from a set of diagrams to the elements of a graph.

Computing filtrations f_i . We compute our family of k vertex-based filtrations using $\Phi: \mathbb{R}^d \rightarrow \mathbb{R}^k$, an MLP with a single hidden layer, such that $f_i := \pi_i \circ \Phi$, i.e. the projection of Φ to the i th dimension. We apply Φ to the hidden representations $x^{(v)}$ of all vertices in the graph.

Embedding function and output. We treat persistence diagrams in dimension 0 and 1 differently. For dimension 0, we have a bijective mapping of tuples in the persistence diagram to the vertices of the graph, which was previously exploited in topological representation learning (Moor et al., 2020). Therefore, we aggregate $\Psi^{(0)}$ with the original node attribute vector $x^{(v)}$ of the graph in a residual fashion, i.e.

$\tilde{x}^{(v)} = x^{(v)} + \Psi^{(0)}(\mathcal{D}_1^{(0)}, \dots, \mathcal{D}_k^{(0)})[v]$, where $\Psi^{(0)}[v]$ denotes that we take the v th row of $\Psi^{(0)}$ (i.e the topological embedding of vertex v). The output of our layer for dimension 0 therefore results in a new representation $\tilde{x}^{(v)} \in \mathbb{R}^d$ for each vertex v , making it compatible with any subsequent (GNN) layers. By contrast, $\Psi^{(1)}$ is pooled into a graph-level representation, to be used in the final classification layer of a GNN. This is necessary because there is no bijective mapping to the vertices, but rather to edges. Yet, it was shown that the precise selection of edges that give rise to topological features can be unstable (Bendich et al., 2020), so we consider it more stable to have this information available *only* on the graph level. For further details, please refer to Section B.3.

Computational complexity. Persistent homology can be calculated efficiently for dimensions 0 and 1, requiring a worst-case complexity of $\mathcal{O}(m\alpha(m))$ for a graph with m sorted edges, where $\alpha(\cdot)$ is the extremely slow-growing inverse Ackermann function, which can be treated as constant for all intents and purposes. The calculation of \mathbf{ph} is therefore dominated by the complexity of sorting all edges, i.e. $\mathcal{O}(m \log m)$, making our approach efficient and scalable. Higher-dimensional persistent homology calculations unfortunately do *not* scale well, having a worst-case complexity of $\mathcal{O}(m^d)$ for calculating d -dimensional topological features, which is why we restrict ourselves to $l = 1$ here.

Limitations. Our approach is practically limited to connected components and cycles. Moreover, our filtrations are incapable of assessing the impact of feature interactions on the topology; for this, we would have to learn *multifiltrations* (Carlsson et al., 2009), but multifiltrations do not afford a concise, efficient representation as the scalar-valued filtrations discussed in this paper. We therefore leave their treatment for future work.

3.1. Choosing an Embedding Function Ψ

The embedding function Ψ influences the resulting representation of the persistence diagrams calculated by our approach. It is therefore crucial to pick a class of functions that are sufficiently powerful to result in expressive representations of a persistence diagram \mathcal{D} . We consider multiple types of embedding functions Ψ , namely (i) a novel approach based on DeepSets (Zaheer et al., 2017), (ii) the *rational hat* function introduced by Hofer et al. (2019), as well as (iii) the triangle point transformation, (iv) the Gaussian point transformation, and (v) the line point transformation, with the last three transformations being introduced in Carrière et al. (2020). Except for the deep sets approach, all of these transformations are *local* in that they apply to a single point in a persistence diagram without taking the other points into account. These functions can therefore be decomposed as $\Psi^{(j)}(\mathcal{D}_1^{(j)}, \dots, \mathcal{D}_k^{(j)})[v] = \tilde{\Psi}^{(j)}(\mathcal{D}_1^{(j)}[v], \dots, \mathcal{D}_k^{(j)}[v])$ for an index v . By contrast, the deep sets approach uses all tuples in the persistence diagrams to compute embeddings.

3.2. Differentiability

The right choice of Ψ will lead to a differentiable downstream representation. It is not a priori clear whether the map $\mathbf{ph}(\cdot)$ is differentiable. This was answered in the affirmative (Gameiro et al., 2016; Hofer et al., 2020; Moor et al., 2020; Poulenard et al., 2018), provided the filtration satisfies injectivity at the vertices. We have the following theorem, whose proof is due to Hofer et al. (2020, Lemma 1).

Theorem 1. *Let f be a vertex filtration function $f: V \rightarrow \mathbb{R}$ with continuous parameters θ , and let Ψ be a differentiable embedding function of unspecified dimensions. If the vertex function values of f are distinct for a specific set of parameters θ' , i.e. $f(v) \neq f(w)$ for $v \neq w$, then the map $\theta \mapsto \Psi(\mathbf{ph}(G, f))$ is differentiable at θ' .*

This theorem is the basis for TOGL, as it states that the filtrations, and thus the resulting ‘views’ on a graph G , can be trained end-to-end. While Hofer et al. (2020) describe this for a *single* filtration, their proof can be directly extended to multiple filtrations as used in our approach.

3.3. Expressive Power

The expressive power of graph neural networks is well-studied (Xu et al., 2019; Morris et al., 2019; Chen et al., 2020; Maron et al., 2019) and typically related back to the Weisfeiler-Lehman¹ iterative label refinement scheme, denoted as WL[1]. Given a graph with an initial set of vertex labels, WL[1] collects the labels of neighbouring vertices for each vertex in a multiset and ‘hashes’ them into a new label (using a perfect hashing scheme so that vertices with the same labels and coinciding neighbourhoods always end up with the same label). This procedure is repeated and stops either when a maximum number of iterations has been reached or no more label updates happen. The result of each iteration h of the algorithm for a graph G is a feature vector $\phi_G^{(h)}$ that contains individual label counts.

Originally meant as a test for graph isomorphism (Weisfeiler & Lehman, 1968), WL[1] has been used in the context of graph classification (Shervashidze & Borgwardt, 2009). The test runs in polynomial time, but is known to fail to distinguish between certain graphs, i.e. there are graphs G and G' , with $G \neq G'$, that obtain the same labelling by WL[1] (Arvind et al. (2019); Fürer (2017)). Surprisingly, Xu et al. (2019) showed that standard graph neural networks based on message passing are *no more powerful* than WL[1]. Higher-order refinement schemes, which pass information over edges ($k = 2$), for instance, can be defined (Maron et al., 2019; Morris et al., 2019). These variants, are strictly more powerful—in that they can distinguish between more classes of graphs—but also computationally more expensive. To prove the expressivity of our method, we will show that it (i) can distinguish all the graphs WL[1] can distinguish, and (ii) that there are graphs that WL[1] cannot distinguish but our method can. We stress that the higher expressivity is not meant to indicate that our approach will perform generally better! In fact, WL[1]

and, by extension, GNNs, are capable of identifying almost all (in the probabilistic sense) non-isomorphic graphs (Babai & Kucera, 1979; Babai et al., 1980). However, the difference in expressivity implies that our method may capture features that cannot be captured by GNNs. Since persistent homology is an isomorphism invariant, we only have to show that we distinguish the same graphs that WL[1] distinguishes.

Theorem 2. *Persistent homology is at least as expressive as WL[1], i.e. if the WL[1] label sequences for two graphs G and G' diverge, the corresponding persistence diagrams \mathcal{D} and \mathcal{D}' are not equal.*

Proof. Assume that the label sequences of G and G' diverge at iteration h . Thus, $\phi_G^{(h)} \neq \phi_{G'}^{(h)}$ and there exists at least one label whose count is different. Let $\mathcal{L}^{(h)} := \{l_1, l_2, \dots\}$ be an enumeration of the finitely many hashed labels at iteration h . We can build a valid filtration function f by assigning a vertex v with label l_i to its index, i.e. $f(v) := i$, and setting $f(v, w) := \max\{f(v), f(w)\}$ for an edge (v, w) . The resulting 0-dimensional persistence diagram \mathcal{D}_0 will contain tuples of the form (i, j) , and each vertex is guaranteed to give rise to *exactly* one such pair. Letting $\mu_0^{(i,j)}(\mathcal{D}_0)$ refer to the multiplicity of a tuple in \mathcal{D}_0 , we know that, since the label count is different, there is *at least* one tuple (k, l) with $\mu_0^{(k,l)}(\mathcal{D}) \neq \mu_0^{(k,l)}(\mathcal{D}')$. Hence, $\mathcal{D} \neq \mathcal{D}'$. \square

There are certain pairs of graphs G, G' that cannot be distinguished by WL[1]. Specifically, let G be a graph consisting of the disjoint union of two triangles, i.e. , and let G' be a graph consisting of a hexagon, i.e. . WL[1] will be unable to distinguish these two graphs because all multisets in every iteration will be the same. Persistent homology, by contrast, can distinguish G from G' by virtue of their Betti numbers. We have $\beta_0(G) = \beta_1(G) = 2$, because G consists of two connected components and two cycles, whereas $\beta_0(G') = \beta_1(G') = 1$ as G' only consists of one connected component and one cycle. Hence, the characteristics captured by persistent homology are different from the ones captured by WL[1], and we can expect topological features to *enrich* the expressivity of WL[1].

Together with Theorem 2, this example implies that persistent homology is *strictly* more powerful than WL[1], although the constructiveness of the proof makes it clear that the expressive power hinges on the expressive power of the filtration—making it crucial that this representation is learned, as our approach does. Since persistent homology can also incorporate higher-order connectivity information such as cliques, we present an extended expressivity analysis in Appendix A.

4. Related Work

Graph representation learning is a topic that has received a large amount of attention by the machine learning community. *Graph kernel methods* address graph classification via (implicit or explicit) embeddings in Reproducing Kernel Hilbert Spaces (Borgwardt et al., 2020; Kriege et al., 2020; Nikolentzos et al., 2019). While powerful and expressive, they cannot capture partial similarities between neighbourhoods. This

¹Multiple spellings are commonplace, and no consensus has been reached in literature.

can be achieved by *graph neural networks*, which typically employ message passing on graphs to learn hidden representations of graph structures and the graphs themselves (Kipf & Welling, 2017; Wu et al., 2021). Recent work in this domain is abundant and includes attempts to include additional substructures (Bouritsas et al., 2021) as well as defining higher-order message passing schemes (Morris et al., 2019).

Our approach falls into the realm of topological data analysis (Edelsbrunner & Harer, 2010) and employs *persistent homology*, a technique for calculating topological features—such as connected components and cycles—of structured data sets. These features are known to be highly characteristic, leading to successful topology-driven machine learning approaches (Hofer et al., 2017, 2020; Moor et al., 2020; Rieck et al., 2019; Zhao & Wang, 2019). At its core of these approaches is the notion of a *filtration*, i.e. a sequence of nested subgraphs (or simplicial complexes in a higher-dimensional setting). Choosing the right filtration is crucial for obtaining good performance. This used to be a daunting task because persistent homology calculations are inherently discrete. Recent advances in proving differentiability enable proper end-to-end training of persistent homology, thus opening the door for hybrid methods that integrate the somewhat complementary view of topological features to increase their expressivity. Of particular interest is the work by Hofer et al. (2020), who demonstrated that a learned filtration can improve upon a pre-defined one when using a topology-based classification approach. We extend this by developing a fully generic topological neural network layer that can be integrated into *any* GNN architecture to increase its awareness of topological features. Closest to our current work are Zhao et al. (2020), who presented a way to enhance GNNs using topological information. In their framework, topology is only used to provide additional scalar-valued weights for the message passing scheme, and topological features are only calculated over small neighbourhoods. Our approach, being end-to-end differentiable, is much more general and permits the calculation of topological features at all scales—including graph-level features—as well as an integration into arbitrary GNN architectures.

5. Experiments

We showcase the empirical performance of TOGL on a set of synthetic and real-world data sets, with a primary focus on assessing to what extent a topology-based representation can be useful. To this end, we generated synthetic data sets whose classes of graphs can be easily distinguished by humans but not by GNNs.² The real-world data sets, by contrast, serve to illustrate that topological information, as obtained from TOGL, *can* be beneficial for predictive performance. We also prepare a series of experiments that serves as an ablation study to analyse the performance of TOGL in case only topological information is available (whereas many data sets already contain a considerable amount of structural information in their node features alone).

²We leave the question of whether this implies the existence of a fundamentally topology-aware functionality in the visual cortex for future work.

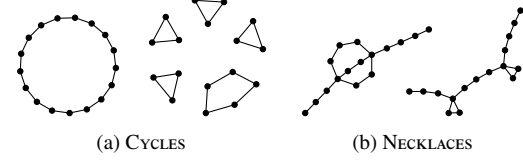


Figure 2.: Example graphs for the synthetic graph classification data sets. The negative class (shown on the left side for each subfigure) and the positive class can be visually distinguished.

5.1. Experimental Setup

Following the setup of Dwivedi et al. (2020), we run our experiments according to a consistent training setup and a limited parameter budget to encourage comparability between architectures. For further details, we refer the interested reader to Appendix C. All experiments were tracked (Biewald, 2020), experimental logs, reports and code will be made publicly available.

Baselines and comparison partners. We compare our method against several baselines : Graph Convolutional Networks (GCN) (Kipf & Welling, 2017), Graph Attention Networks (GAT) (Veličković et al., 2018), Gated-GCN (Bresson & Laurent, 2017), Graph Information Networks (GIN) (Xu et al., 2019), the Weisfeiler–Lehman kernel (WL) (Shervashidze & Borgwardt, 2009) and WL-OA (Kriege et al., 2016). The performance of those have been assessed in benchmarking papers (Dwivedi et al., 2020; Borgwardt et al., 2020; Morris et al., 2020) and experimental conditions between these publications are comparable. We stress that we use the same folds and hyperparameters as in the corresponding benchmarking papers to ensure a fair comparison. Out of all baselines, our main comparison partner is the 4-layer GCN architecture of Dwivedi et al. (2020), which has been shown to give competitive results on many benchmarking tasks. We refer to this method as GCN-4. To assess the benefits of having access to topological information, we replace the second layer of GCN-4 by TOGL. Thus, our method has approximately the same number of parameters than GCN-4, but can make use of topological information, which is subsequently used in other graph convolutional layers. We refer to this architecture as TopoGNN-3-1.

Embedding functions. The choice of the embedding function is used as an hyperparameter in our training. In Section 5.5, we provide a comprehensive assessment of the difference between the DeepSets approach (which is capable of capturing *interactions* between tuples in a persistence diagram) and decomposed embedding functions which do not account for interactions.

Ablated static variant of TOGL. We also developed an ablated static variant of our layer, serving as a comparison partner that mimics the calculation of a filtration in terms of the number of parameters but *without* taking topological

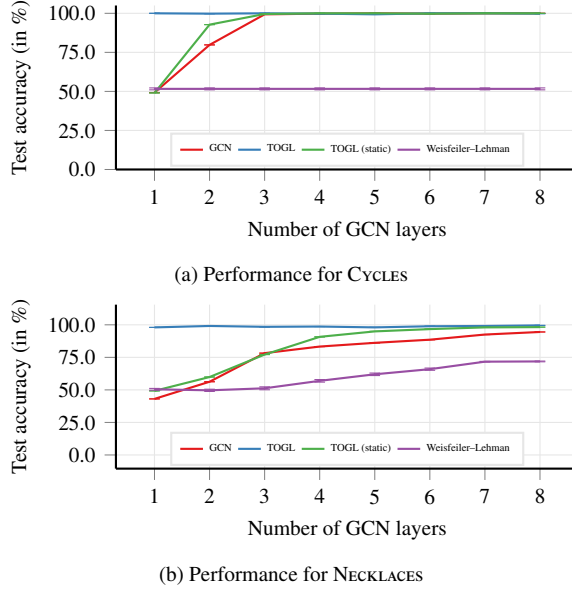


Figure 3.: Performance comparison on synthetic data sets as a function of the number of GCN layers.

features into account. The layer uses a *static* mapping (instead of a dynamic one based on persistent homology) of vertices to themselves (for dimension 0), and employs a random edge selection process (for dimension 1). This has the effect of learning graph-level information that is not strictly based on topology but on node feature values. The static variant of TOGL reduces to an MLP that is applied per vertex in case interactions between tuples are not regarded, and to the application of a DeepSet Zaheer et al. (2017) to the vertex representations if interactions between tuples are incorporated. Generally, if the static variant performs well on a data set, we assume that performance is driven much more by the availability of *any* graph-level type of information, such as the existence of certain nodes or groups of nodes, as opposed to topological information.

5.2. Synthetic Data Sets

We generate two synthetic balanced 2-class data sets of 1000 graphs each. In the CYCLES data set (Figure 2a), we generate either one large cycle (class 0) or multiple small ones (class 1). These graphs can be easily distinguished by *any* topological approach because they differ in the number of connected components and the number of cycles. For the NECKLACES data set (Figure 2b), we generate ‘chains’ of vertices with either two individual cycles, or a ‘merged’ one. From the point of topology, both classes have the same *number* of cycles, but the incorporation of additional neighbourhood information—via a GNN, for instance—will make them distinguishable for TOGL, thus showcasing the power of a hybrid method.

As Figure 3a indicates, the CYCLES data set can be easily distinguished by TOGL. Even with only a single GCN layer in addition to our layer, we obtain almost perfect classification performance. To classify this data set properly with a

standard GCN, we need at least four layers. The Weisfeiler–Lehman subtree graph kernel, i.e. WL[1], with the number of iterations h being equivalent to the number of layers, cannot classify this data set correctly based on the input degree sequences, thus showcasing the benefits of having access to a learnable node representation, which the GCN can use to improve its performance (given enough layers).

For the NECKLACES data, we also observe that TOGL performs well regardless of the depth of the network. Since the graphs in the NECKLACES data set cannot be easily distinguished by connected component information alone, having access to cycle information is crucial. We also observe that a standard GCN requires a large number of layers to even approach our performance. A similar effect can be seen for WL[1], whose performance is not on a par with a GCN on this data set and plateaus for $h \geq 7$. On both data sets, the static variant is performing better than the standard GCN, but *significantly worse* than the classical TOGL, due to its very limited access to topological information.

5.3. Benchmark Data Sets

Having ascertained the general utility of TOGL for classifying data sets with topological information, we now analyse the effects of TOGL in graph classification tasks. Table 1 depicts the results on well-known benchmark data sets. Except for the ENZYMES data set, we observe a beneficial effect of TOGL overall. Indeed, TOGL performs on a par with GCN-4, and even exhibits a slight improvement for DD and IMDB-BINARY. These results suggest that, even in cases where topological features might not be informative, one TOGL layer can achieve at least the same *relative* performance increase as a GCN layer. As for the performances on ENZYMES, we experience a severe level of overfitting during model training. This is exacerbated by the fact that ENZYMES is the smallest of the compared datasets and we eschewed the tuning of regularisation hyperparameters (such as ‘dropout’), for the sake of having a fair comparison with the setup of Dwivedi et al. (2020).

Overall, there are no scenarios in which the integration of topological information leads to a decisive improvement in performance. In a similar fashion, our static approach, which employs a comparatively simple filtration and edge selection process as described above, is competitive with TOGL, and even approaches GCN-4 performance on REDDIT-BINARY. This behaviour indicates that predictive performance is *not* driven by having access to topological information on the benchmark data sets. To some extent, this is surprising, as some of the data sets turn out to contain numerous salient topological features by visual inspection alone (Figure S5), whereas the social networks exhibit more community-like behaviour (Figure S6).

5.4. Artificially Generated Graphs

To further elucidate the inclusion of topological features using our layer on larger data sets, we also compare to two graph classification datasets which were generated from image superpixels (MNIST, CIFAR10) and two node classification

Table 1.: Test accuracy on real-world benchmark data sets. Methods printed in black have been run in our setup, while methods printed in grey are cited from the literature, whenever available. For PROTEINS-FULL, ENZYMEs and DD, we use values reported by Dwivedi et al. (2020). For IMDB-BINARY and REDDIT-BINARY, we use numbers reported by Morris et al. (2020), whereas for WL and WL-OA (Kriege et al., 2016), we make use of a recent survey (Borgwardt et al., 2020). GIN-4 results marked with a '*' are 1 layer GIN- ϵ as reported in Morris et al. (2020).

METHOD	PROTEINS-FULL	ENZYMEs	DD	IMDB-BINARY	REDDIT-BINARY
GAT-4	76.3 ± 2.4	68.5 ± 5.2	75.9 ± 3.8	N.A.	N.A.
GATED-GCN-4	76.4 ± 2.9	65.7 ± 4.9	72.9 ± 2.1	N.A.	N.A.
GCN-4	76.1 ± 2.4	65.8 ± 4.6	72.8 ± 4.1	68.6 ± 4.9	92.8 ± 1.7
GIN-4	74.1 ± 3.4	65.3 ± 6.8	71.9 ± 3.9	$72.9 \pm 4.7^*$	$89.8 \pm 2.2^*$
TopoGNN-3-1	76.0 ± 3.9	53.0 ± 9.2	73.2 ± 4.7	72.0 ± 2.3	89.4 ± 2.2
TopoGNN-3-1 (static)	75.7 ± 3.6	49.8 ± 7.0	71.0 ± 2.8	72.8 ± 5.4	92.1 ± 1.6
WL	73.1 ± 0.5	54.3 ± 0.9	77.7 ± 2.0	71.2 ± 0.5	78.0 ± 0.6
WL-OA	73.5 ± 0.9	58.9 ± 0.9	77.8 ± 1.2	74.0 ± 0.7	87.6 ± 0.3

Table 2.: Test accuracy on image and SBM-based benchmark data sets. Methods printed in black have been run in our setup, while methods printed in grey are cited from Dwivedi et al. (2020). Our results on GCN-4 differ slightly due to a known misalignment in their implementation with the original GCN architecture. We report weighted accuracy on CLUSTER and PATTERN.

METHOD	MNIST	CIFAR-10	CLUSTER	PATTERN
GAT-4	95.5 ± 0.2	64.2 ± 0.4	57.7 ± 0.3	75.8 ± 1.8
GATED-GCN-4	97.3 ± 0.1	67.3 ± 0.3	60.4 ± 0.4	84.5 ± 0.1
GIN-4	96.5 ± 0.3	55.5 ± 1.5	58.4 ± 0.2	85.6 ± 0.0
GCN-4	90.0 ± 0.3	54.2 ± 1.5	57.0 ± 0.9	85.5 ± 0.4
TopoGNN-3-1	95.5 ± 0.2	61.7 ± 1.0	60.4 ± 0.2	86.6 ± 0.1
TopoGNN-3-1 (static)	95.4 ± 0.1	62.1 ± 0.5	60.5 ± 0.2	85.6 ± 0.1

datasets (CLUSTER and PATTERN) which were generated using Stochastic Block Models (SBM), all four of which were introduced in Dwivedi et al. (2020). Table 2 depicts the results. Interestingly, much of the improvement of our approach can be attributed to the additional node level transformations and *not* to the inclusion of topological information, which is shown by similar performance of our method and its static variant. Only on PATTERN we see that topological information improves the performance of the model to a significant degree, with the static variant performing similar to a GCN.

This is in line with our expectations, as the image based data sets contain very little topological structure; each node represents a superpixel of the original image, which is connected to the k -nearest neighbours in the image domain, leading to a highly regular graph structure. By contrast, we expect more topological information to be present in the SBM data sets, which aligns with our observations for PATTERN.

5.5. Structure-Based Classification of Molecular Graphs

A recent survey (Borgwardt et al., 2020) showed that the node features of these graphs already carry substantial information,

which often makes even simple histogram-based approaches perform comparatively well. This motivated us to prepare another set of experiments, in which we classify molecular graphs based on graph shape/structure information alone. We therefore removed all existing node labels and node features from DD, ENZYMEs, PROTEINS-FULL, and MNIST replacing them by random features, and adding a suffix of -STRUCT to their name to indicate this change. This leaves only graph structure information for the classification. We also use this setup as an ablation study to assess the relative importance of the static architecture and the embedding function variants, i.e. deep sets versus known embedding functions for persistence diagrams.

Figure 4 and Figure S7 depict the results of several models for different number of GCN layers. We observe a *clear advantage* of TOGL over its static counterparts, confirming the importance of the ability of TOGL to extract topological information. The difference between the interacting and non-interacting embedding functions is not significant and suggests that allowing for interactions between the persistence tuples is not strictly beneficial. Finally, TOGL (in its non-static version) clearly outperforms the GCN baseline. Numerical results for these experiments are listed in Table S6.

6. Conclusion

We presented TOGL, a generically-applicable layer that incorporates topological information into any GNN architecture. On benchmark data sets, we observe that our topology-aware approach can help improve predictive performance. Interestingly, *both* our method and its static ablated variant perform similarly when classification performance does not appear to rely on topological features. On data sets with pronounced topological structures, by contrast, we find that our method helps a GCN achieve excellent performance. We observe that topological information sometimes also leads to overfitting issues on smaller data sets, and leave the investigation of additional regularisation strategies for our method for future work. Moreover, we hypothesise that the use of different filtrations (Milosavljević et al., 2011) and improved persistent

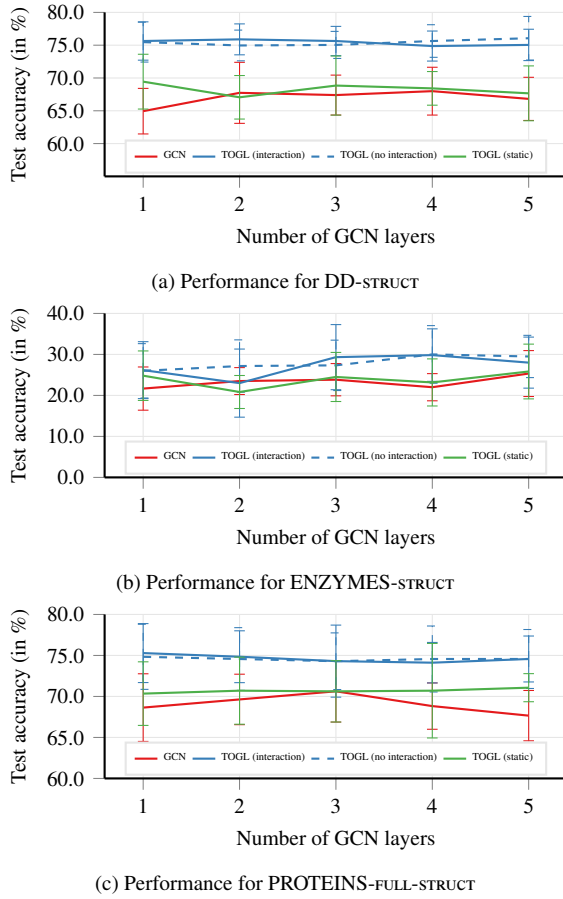


Figure 4.: Comparison of test accuracy for the structure-based variants of the benchmark data sets while varying network depth, i.e. the number of GCN layers. Error bars denote the standard deviation of test accuracy over 10 cross-validation folds. *Interaction* refers to using a DeepSets approach for embedding persistence diagrams, whereas *no interaction* uses persistence diagrams coordinate functions that do not account for pairwise interactions.

homology algorithms (Cohen-Steiner et al., 2009), which pair *all* topological features, will prove beneficial.

Acknowledgements

The authors thank Weights and Biases, Inc., for providing us with a free academic team account. This project was supported by the grant #2017-110 of the Strategic Focal Area “Personalized Health and Related Technologies (PHRT)” of the ETH Domain for the SPHN/PHRT Driver Project “Personalized Swiss Sepsis Study” and the Alfred Krupp Prize for Young University Teachers of the Alfred Krupp von Bohlen und Halbach-Stiftung (K.B.) Edward De Brouwer gratefully acknowledges support by an FWO-SB grant and support from NVIDIA for GPUs. Yves Moreau is funded by (1) Research Council KU Leuven: C14/18/092 Sym-

BioSys3; CELSA-HIDUCTION, (2) Innovative Medicines Initiative: MELLODY, (3) Flemish Government (ELIXIR Belgium, IWT, FWO 06260) and (4) Impulsfonds AI: VR 2019 2203 DOC.0318/1QUATER Kenniscentrum Data en Maatschappij. Some computational resources and services used in this work were provided by the VSC (Flemish Supercomputer Center), funded by the Research Foundation - Flanders (FWO) and the Flemish Government – department EWI.

References

Arvind, V., Fuhlbrück, F., Köbler, J., and Verbitsky, O. On Weisfeiler–Leman invariance: Subgraph counts and related graph properties. In *Fundamentals of Computation Theory*, pp. 111–125, Cham, Switzerland, 2019. Springer.

Babai, L. and Kucera, L. Canonical labelling of graphs in linear average time. In *20th Annual Symposium on Foundations of Computer Science*, pp. 39–46, 1979.

Babai, L., Erdős, P., and Selkow, S. M. Random graph isomorphism. *SIAM Journal on Computing*, 9(3):628–635, 1980.

Barannikov, S. A. The framed Morse complex and its invariants. *Advances in Soviet Mathematics*, 21:93–115, 1994.

Bendich, P., Bubenik, P., and Wagner, A. Stabilizing the unstable output of persistent homology computations. *Journal of Applied and Computational Topology*, 4(2):309–338, June 2020.

Biewald, L. Experiment tracking with weights and biases, 2020. URL <https://www.wandb.com/>. Software available from wandb.com.

Borgwardt, K., Ghisu, E., Llinares-López, F., O’Bray, L., and Rieck, B. Graph kernels: State-of-the-art and future challenges. *Foundations and Trends® in Machine Learning*, 13(5–6):531–712, 2020.

Bouritsas, G., Frasca, F., Zafeiriou, S., and Bronstein, M. M. Improving graph neural network expressivity via subgraph isomorphism counting, 2021.

Bresson, X. and Laurent, T. Residual gated graph convnets. *arXiv preprint arXiv:1711.07553*, 2017.

Carlsson, G., Singh, G., and Zomorodian, A. Computing multidimensional persistence. In *International Symposium on Algorithms and Computation (ISAAC)*, pp. 730–739, Heidelberg, Germany, 2009. Springer.

Carrière, M., Chazal, F., Ike, Y., Lacombe, T., Royer, M., and Umeda, Y. Perslay: a neural network layer for persistence diagrams and new graph topological signatures. In *International Conference on Artificial Intelligence and Statistics*, pp. 2786–2796. PMLR, 2020.

Carrière, M., Chazal, F., Ike, Y., Lacombe, T., Royer, M., and Umeda, Y. PersLayer: A neural network layer for persistence diagrams and new graph topological signatures. In *Proceedings of the 23rd International Conference on Artificial Intelligence and Statistics (AISTATS)*, volume 108 of *Proceedings of Machine Learning Research*, pp. 2786–2796. PMLR, 2020.

Cavanna, N. J., Jahanseir, M., and Sheehy, D. R. Visualizing sparse filtrations. In *Proceedings of the 31st International Symposium on Computational Geometry*, 2015a.

Cavanna, N. J., Jahanseir, M., and Sheehy, D. R. A geometric perspective on sparse filtrations. In *Proceedings of the Canadian Conference on Computational Geometry*, 2015b.

Chen, Z., Chen, L., Villar, S., and Bruna, J. Can graph neural networks count substructures?, 2020.

Cohen-Steiner, D., Edelsbrunner, H., and Harer, J. Extending persistence using Poincaré and Lefschetz duality. *Foundations of Computational Mathematics*, 9(1):79–103, February 2009.

Dwivedi, V. P., Joshi, C. K., Laurent, T., Bengio, Y., and Bresson, X. Benchmarking graph neural networks, 2020.

Edelsbrunner, H. and Harer, J. *Computational topology: An introduction*. American Mathematical Society, Providence, RI, USA, 2010.

Edelsbrunner, H., Letscher, D., and Zomorodian, A. J. Topological persistence and simplification. *Discrete & Computational Geometry*, 28(4):511–533, November 2002.

Fürer, M. On the combinatorial power of the weisfeiler-lehman algorithm. In *Algorithms and Complexity*, pp. 260–271, Cham, Switzerland, 2017. Springer.

Gameiro, M., Hiraoka, Y., and Obayashi, I. Continuation of point clouds via persistence diagrams. *Physica D: Nonlinear Phenomena*, 334:118–132, 2016. Topology in Dynamics, Differential Equations, and Data.

Hatcher, A. *Algebraic topology*. Cambridge University Press, Cambridge, England, 2002.

Hofer, C., Kwitt, R., Niethammer, M., and Uhl, A. Deep learning with topological signatures. In *Advances in Neural Information Processing Systems 30 (NeurIPS)*, pp. 1634–1644. Curran Associates, Inc., Red Hook, NY, USA, 2017.

Hofer, C. D., Kwitt, R., and Niethammer, M. Learning representations of persistence barcodes. *Journal of Machine Learning Research*, 20(126):1–45, 2019.

Hofer, C. D., Graf, F., Rieck, B., Niethammer, M., and Kwitt, R. Graph filtration learning. In *Proceedings of the 37th International Conference on Machine Learning (ICML)*, volume 119 of *Proceedings of Machine Learning Research*, pp. 4314–4323. PMLR, 2020.

Kim, K., Kim, J., Zaheer, M., Kim, J. S., Chazal, F., and Wasserman, L. Plplay: Efficient topological layer based on persistence landscapes, 2021.

Kipf, T. N. and Welling, M. Semi-supervised classification with graph convolutional networks. In *Proceedings of the 5th International Conference on Learning Representations (ICLR)*, 2017.

Kriege, N. M., Giscard, P.-L., and Wilson, R. On valid optimal assignment kernels and applications to graph classification. In *Advances in Neural Information Processing Systems 29*, pp. 1623–1631. Curran Associates, Inc., 2016.

Kriege, N. M., Johansson, F. D., and Morris, C. A survey on graph kernels. *Applied Network Science*, 5(1):6, 2020.

Maron, H., Ben-Hamu, H., Serviansky, H., and Lipman, Y. Provably powerful graph networks. In Wallach, H., Larochelle, H., Beygelzimer, A., d’Alché-Buc, F., Fox, E., and Garnett, R. (eds.), *Advances in Neural Information Processing Systems 32*, pp. 2156–2167. Curran Associates, Inc., 2019.

McKay, B. D. and Spence, E. Classification of regular two-graphs on 36 and 38 vertices. *Australasian Journal of Combinatorics*, 24:293–300, 2001.

Milosavljević, N., Morozov, D., and Skraba, P. Zigzag persistent homology in matrix multiplication time. In *Proceedings of the 27th Annual Symposium on Computational Geometry (SoCG)*, pp. 216–225, 2011.

Moor, M., Horn, M., Rieck, B., and Borgwardt, K. Topological autoencoders. In *Proceedings of the 37th International Conference on Machine Learning (ICML)*, volume 119 of *Proceedings of Machine Learning Research*, pp. 7045–7054. PMLR, 2020.

Morris, C., Ritzert, M., Fey, M., Hamilton, W. L., Lenssen, J. E., Rattan, G., and Grohe, M. Weisfeiler and Leman go neural: Higher-order graph neural networks. *Proceedings of the AAAI Conference on Artificial Intelligence*, 33(01):4602–4609, July 2019.

Morris, C., Kriege, N. M., Bause, F., Kersting, K., Mutzel, P., and Neumann, M. Tudataset: A collection of benchmark datasets for learning with graphs, 2020.

Nikolentzos, G., Siglidis, G., and Vazirgiannis, M. Graph kernels: a survey, 2019.

Poulenard, A., Skraba, P., and Ovsjanikov, M. Topological function optimization for continuous shape matching. *Computer Graphics Forum*, 37(5):13–25, 2018.

Rieck, B., Bock, C., and Borgwardt, K. A persistent Weisfeiler–Lehman procedure for graph classification. In *Proceedings of the 36th International Conference on Machine Learning*, volume 97, pp. 5448–5458. PMLR, June 2019.

Sheehy, D. R. Linear-size approximations to the Vietoris–Rips filtration. *Discrete & Computational Geometry*, 49(4):778–796, 2013.

Shervashidze, N. and Borgwardt, K. Fast subtree kernels on graphs. In *Proceedings of the 22nd International Conference on Neural Information Processing Systems*, pp. 1660–1668, USA, 2009. Curran Associates Inc.

Veličković, P., Cucurull, G., Casanova, A., Romero, A., Liò, P., and Bengio, Y. Graph attention networks. In *International Conference on Learning Representations*, 2018.

Verri, A., Uras, C., Frosini, P., and Ferri, M. On the use of size functions for shape analysis. *Biological Cybernetics*, 70(2):99–107, December 1993.

Weisfeiler, B. and Lehman, A. A. The reduction of a graph to canonical form and the algebra which appears therein. *Nauchno–Technicheskaja Informatsija*, 9:12–16, 1968.

Wu, Z., Pan, S., Chen, F., Long, G., Zhang, C., and Yu, P. S. A comprehensive survey on graph neural networks. *IEEE Transactions on Neural Networks and Learning Systems*, 32(1):4–24, 2021.

Xu, K., Hu, W., Leskovec, J., and Jegelka, S. How powerful are graph neural networks? In *International Conference on Learning Representations*, 2019.

Zaheer, M., Kottur, S., Ravanbakhsh, S., Poczos, B., Salakhutdinov, R. R., and Smola, A. J. Deep sets. In *Advances in Neural Information Processing Systems*, volume 30, pp. 3391–3401. Curran Associates, Inc., 2017.

Zhao, Q. and Wang, Y. Learning metrics for persistence-based summaries and applications for graph classification. In *Advances in Neural Information Processing Systems 32 (NeurIPS)*, pp. 9855–9866. Curran Associates, Inc., 2019.

Zhao, Q., Ye, Z., Chen, C., and Wang, Y. Persistence enhanced graph neural network. In *Proceedings of the 23rd International Conference on Artificial Intelligence and Statistics (AISTATS)*, volume 108 of *Proceedings of Machine Learning Research*, pp. 2896–2906. PMLR, 26–28 Aug 2020.

Zomorodian, A. J. Fast construction of the Vietoris–Rips complex. *Computers & Graphics*, 34(3):263–271, 2010.

A. Analysis of (Strongly) Regular Graphs

A *k-regular graph* is a graph $G = (V, E)$ in which all vertices have degree k . For $k = \{3, 4\}$, such graphs are also known as cubic and quartic graphs, respectively. The Weisfeiler–Lehman test is capable of distinguishing between certain variants of these graphs (even though we observe that WL[1] is not sufficient to do so). Similarly, a *strongly regular* graph is a graph $G = (V, E)$ with two integers $\lambda, \mu \in \mathbb{N}$ such that each pair of adjacent vertices has λ common neighbours, whereas every pair of non-adjacent vertices has μ common neighbours.

Persistent homology can make use of higher-order connectivity information to distinguish between these data sets. To demonstrate this, we use a standard degree filtration and compute persistent homology of the graph, including all higher-order cliques. We then calculate the *total persistence* of each persistence diagram \mathcal{D} , and use it to assign a feature vector to the graph. This is in some sense the simplest way of employing persistent homology; notice that we are *not* learning a new filtration but keep a fixed one. Even in this scenario, we find that there is always a significant number of pairs of graphs whose feature vectors do not coincide—or, conversely speaking, as Table S3 shows, there are only between 14%–22% of pairs of graphs that we cannot distinguish by this simple scheme. This illustrates the general expressivity that a topology-based perspective can yield. For the strongly-regular graphs, we observe even lower error rates: we only fail to distinguish about 1.2% of all pairs (specifically, 8236 out of 7424731 pairs) of the 3854 strongly-regular graphs on 35 vertices with $\lambda = \mu = 9$ (McKay & Spence, 2001).

A note on computational complexity. At the same time, this approach is also not without its disadvantages. Since we perform a clique counting operation, the complexity of the calculation increases considerably, and we would not suggest to use persistent homology of arbitrary dimensions in practice. While there are some algorithmic improvements in topological constructions (Zomorodian, 2010), naïve persistent homology calculations of arbitrary order may quickly become infeasible for larger data sets. This can be alleviated to a certain extent by *approximating* persistent homology (Cavanna et al., 2015a,b; Sheehy, 2013), but the practical benefits of this are unclear. Nevertheless, this experiment should therefore be considered as an indication of the utility of topological features in general to complement and enhance existing architectures.

B. Topological Data Analysis

We provide a more formal introduction to persistent homology, the technique on which TOGL is fundamentally based. Persistent homology arose as one of the flagship approaches in the field of computational topology, which aims to make methods from this highly abstract branch of mathematics available for data analysis purposes.

To gain a better understanding, we will briefly take a panoramic tour through algebraic topology, starting from *simplicial homology*, an algebraic technique for ‘calculating’ the connectivity of topological spaces, represented in the form

Table S3.: Error rates when using persistent homology with a degree filtration to classify pairs of k -regular on n vertices. r3-n12 denotes 3-regular graphs on 12 vertices, for instance. This list is by no means exhaustive, but indicates the general utility of persistent homology and its filtration-based analysis.

Data set	Graphs	Pairs	Error	Error rate
r3-n12	85	3570	712	19.94%
r3-n14	509	129286	26745	20.69%
r3-n16	4060	8239770	1757385	21.33%
r4-n10	59	1711	229	13.38%
r4-n11	265	34980	4832	13.81%
r4-n12	1544	1191196	170814	14.34%

of simplicial complexes, i.e. generalised graphs. Simplicial homology is said to assess the connectivity of a topological space by ‘counting its high-dimensional holes’. We will see how to make this description more precise.

B.1. Simplicial Homology

Simplicial complexes are the central concept in algebraic topology. A simplicial complex K consists of a set of *simplices* of certain dimensions, such as vertices (dimension 0), edges (dimension 1), and triangles (dimension 2). Each simplex $\sigma \in K$ has a set of faces, and each face τ has to satisfy $\tau \in K$. Moreover, if $\sigma \cap \sigma' \neq \emptyset$ for $\sigma, \sigma' \in K$, then $\sigma \cap \sigma' \in K$. Thus, K is ‘closed under calculating the faces of a simplex’. A graph can be seen as a low-dimensional simplicial complex that only contains 0-simplices (vertices) and 1-simplices (edges), so everything we say applies, *mutatis mutandis*, also to graphs.

Chain groups. For a simplicial complex K , we denote by $C_d(K)$ the vector space generated over \mathbb{Z}_2 (the field with two elements). The elements of $C_d(K)$ are the d -simplices in K , or rather their *formal sums* with coefficients in \mathbb{Z}_2 . For example, $\sigma + \tau$ is an element of the chain group, also called a *simplicial chain*. Addition is well-defined and easy to implement as an algorithm since a simplex can only be present or absent over \mathbb{Z}_2 coefficients.³ The use of chain groups lies in providing the underlying vector space to formalise boundary calculations over a simplicial complex. The boundary calculations, in turn, are necessary to quantify the connectivity!

Boundary homomorphism. Given a d -simplex $\sigma = (v_0, \dots, v_d) \in K$, we can formalise its face or ‘boundary’ calculation by defining the boundary operator $\partial_d: C_d(K) \rightarrow C_{d-1}(K)$ as a sum of the form

$$\partial_d(\sigma) := \sum_{i=0}^d (v_0, \dots, v_{i-1}, v_{i+1}, \dots, v_d), \quad (3)$$

³Different choices of coefficient fields would be possible, but are rarely used for data analysis purposes.

i.e. we leave out every vertex v_i of the simplex once. Since only sums are involved, this operator is seen to be a homomorphism between the chain groups; the calculation extends to $C_d(K)$ by linearity. The boundary homomorphism gives us a way to precisely define what we understand by connectivity. To this end, note that its *kernel* and *image* are well-defined. The kernel $\ker \partial_d$ contains all d -dimensional simplicial chains that do not have a boundary. We can make this more precise by using a construction from group theory.

Homology groups. The last ingredient for the connectivity analysis involves calculating a special group, the homology group. The d th homology group $H_d(K)$ of K is defined as the *quotient group* $H_d(K) := \ker \partial_d / \text{im } \partial_{d+1}$. The quotient operation can be thought of as calculating a special subset—the kernel of the boundary operator—and then *removing* another subset, namely the image of the boundary operator with an increased dimension. This behoves a short explanation. The main reason behind this operation is that *just* the kernel calculation is insufficient to properly count a hole. For example, if we take the three edges of any triangle, their boundary will always be empty, i.e. they are a part of $\ker \partial_1$. However, if the *interior* of the triangle is also part of the simplicial complex—in other words, if we have the corresponding 2-simplex as well—we should *not* count the edges as a hole. This is why we need to remove all elements in the image of ∂_2 . Coincidentally, this also explains why cycles in a graph never ‘vanish’—there are simply no 2-simplices available since the graph is only a 1-dimensional simplicial complex.

Betti numbers. To fully close the loop, as it were, it turns out that we can calculate Betti numbers from homology groups. Specifically, the *rank* of the d th homology group—in the group-theoretical sense—is precisely the d th Betti number β_d , i.e. $\beta_d(K) := \text{rank } H_d(K)$. The sequence of Betti numbers β_0, \dots, β_d of a d -dimensional simplicial complex is commonly used as a complexity measure, and they can be used to discriminate manifolds. For example, a 2-sphere has Betti numbers $(1, 0, 1)$, while a 2-torus has Betti numbers $(1, 2, 1)$. As we outlined in the main text, Betti numbers are of limited use when dealing with complex graphs, however, because they are very coarse counts of features. It was this limited expressivity that prompted the development of persistent homology.

B.2. Persistent Homology

Persistent homology is an extension of simplicial homology, which employs *filtrations* to imbue a simplicial complex K with scale information. Let us assume the existence of a function $f: K \rightarrow \mathbb{R}$, which only attains a finite number of function values $f^{(0)} \leq f^{(1)} \leq \dots \leq f^{(m-1)} \leq f^{(m)}$. We may now, as in the main text, sort K according to f , leading again to a nested sequence of simplicial complexes

$$\emptyset = K^{(0)} \subseteq K^{(1)} \subseteq \dots \subseteq K^{(m-1)} \subseteq K^{(m)} = K, \quad (4)$$

in which $K^{(i)} := \{\sigma \in K \mid f(\sigma) \leq f^{(i)}\}$, i.e. each subset contains only those simplices whose function value is less than or equal to the threshold. In contrast to simplicial homology,

the filtration holds potentially more information because it can track *changes*! For example, a topological feature might be *created* (a new connected component might arise) or *destroyed* (two connected components might merge into one), as we go from some $K^{(i)}$ to $K^{(i+1)}$. At its core, persistent homology is ‘just’ a way of tracking topological features, representing each one by a creation and destruction value $(f^{(i)}, f^{(j)}) \in \mathbb{R}^2$, with $i \leq j$. In case a topological feature is still present in $K^{(m)} = K$, such as a cycle in a graph, it can also be assigned a tuple of the form $(f^{(i)}, \infty)$. Such tuples constitute *essential features* of a simplicial complex and are usually assigned a large destruction value or treated separately in an algorithm (Hofer et al., 2017). While it is also possible to obtain only tuples with finite persistence values, a process known as *extended persistence* (Cohen-Steiner et al., 2009), we focus only on ‘ordinary’ persistence in this paper because of the lower computational complexity.

Persistent homology groups. The filtration above is connected by the inclusion homomorphism between $K^{(i)} \subseteq K^{(i+1)}$. The respective boundary homomorphisms induce a homomorphism between corresponding homology groups of the filtration, i.e. a map $i_d^{(i,j)}: H_d(K_i) \rightarrow H_d(K_j)$. This family of homomorphisms gives rise to a sequence of homology groups

$$\begin{aligned} H_d(K^{(0)}) &\xrightarrow{i_d^{(0,1)}} H_d(K^{(1)}) \xrightarrow{i_d^{(1,2)}} \dots \xrightarrow{i_d^{(m-2,m-1)}} \\ &\xrightarrow{i_d^{(m-1,m)}} H_d(K^{(m)}) = H_d(K) \end{aligned} \quad (5)$$

for every dimension d . For $i \leq j$, the d th persistent homology group is defined as

$$H_d^{(i,j)} := \ker \partial_d(K^{(i)}) / (\text{im } \partial_{d+1}(K^{(j)}) \cap \ker \partial_d(K^{(i)})). \quad (6)$$

Intuitively, this group contains all homology classes *created* in $K^{(i)}$ that are *also* present in $K^{(j)}$. Similar to the ‘ordinary’ Betti number, we may now define the d th persistent Betti number as the rank of this group, i.e.

$$\beta_d^{(i,j)} := \text{rank } H_d^{(i,j)}. \quad (7)$$

Noting the set of indices i, j , we can see persistent homology as generating a *sequence* of Betti numbers, as opposed to just calculating a single number. This makes it possible for us to describe topological features in more detail, and summarise them in a *persistence diagram*.

Persistence diagrams. Given a filtration induced by a function $f: K \rightarrow \mathbb{R}$ as described above, we store each tuple $(f^{(i)}, f^{(j)})$ with multiplicity

$$\mu_{i,j}^{(d)} := (\beta_d^{(i,j-1)} - \beta_d^{(i,j)}) - (\beta_d^{(i-1,j-1)} - \beta_d^{(i-1,j)}) \quad (8)$$

in the d th persistence diagram \mathcal{D}_d . Notice that for most pairs of indices, $\mu_{i,j}^{(d)} = 0$. Given a point $(x, y) \in \mathcal{D}_d$, we refer to the quantity $\text{pers}(x, y) := |y - x|$ as its *persistence*. The idea of persistence arose in multiple contexts (Barannikov, 1994; Edelsbrunner et al., 2002; Verri et al., 1993), but it is nowadays commonly used to analyse functions on manifolds, where high persistence is seen to correspond to *features* of the function, while low persistence is typically considered *noise*.

Table S4.: Parameters of learning rate scheduling for training of models in this work.

NAME	MNIST, CIFAR, PARTNERS, CLUSTER	PROTEINS, ZYMES, DD
lr_{init}	1×10^{-3}	7×10^{-4}
lr_{min}	1×10^{-5}	1×10^{-6}
$lr_{patience}$	10	25

B.3. Computational details

The cardinality of the persistence diagram of dimension-0, \mathcal{D}_0 is equal to the number of vertices, n in the graph. A natural pairing of persistence tuples then consists in assigning each tuple to the node that generated it. As for dimension-1, \mathcal{D}_1 contains as many tuples as cycles in the graph. However, there is no bijective mapping between dimension-1 persistence tuples and vertices. Rather, we link each dimension-1 tuple to the edge that created that particular cycle. To account for multiple distinct filtrations and because the same cycle can be assigned to different edges depending on the specific filtration function, we define a *dummy* tuple for edges that are not linked to any cycle for a particular filtration. The set of persistence diagrams $(\mathcal{D}_1^{(l)}, \dots, \mathcal{D}_k^{(l)})$ can then be concatenated as a matrix in $\mathbb{R}^{d_l \times 2 \cdot k}$, with $d_l = |V|$ (the number of vertices in graph G) if $l = 0$ and $d_l = |E|$ (the number of edges in G) if $l = 1$. Remarkably, that leads to $\Psi^{(l)}(\mathcal{D}_1^{(l)}, \dots, \mathcal{D}_k^{(l)})$ being an operator on a matrix, significantly facilitating computations.

Because of its natural indexing to the vertices, $\Psi^{(0)}(\mathcal{D}_1^{(0)}, \dots, \mathcal{D}_k^{(0)})$ can be mapped back to the graph as explained in Section 3. For $l = 1$, we pool $\Psi^{(1)}(\mathcal{D}_1^{(1)}, \dots, \mathcal{D}_k^{(1)})$ to a graph-level embedding, and mask out the edge indices that are not assigned a persistence pair in any of the $\mathcal{D}_k^{(1)}$.

C. Experimental setup

Following the setup of Dwivedi et al. (2020), we implemented the following training procedure: All models are initialised with an initial learning rate lr_{init} , which varies between the datasets. During training the loss on the validation split is monitored and the learning rate is halved if the validation loss does not improve over a period of $lr_{patience}$. Runs are stopped when the learning rate gets reduced to a value of lower than lr_{min} . The parameters for the different dataset are shown in Table S4.

D. Hyperparameters

Table S5 contains a listing of all hyperparameters used to train TOGL. For the Weisfeiler–Lehman subtree kernel, which we employed as a comparison partner on the synthetic data sets, we used a support vector machine classifier with a linear kernel, whose regularisation parameter $C \in \{10^{-4}, 10^{-3}, \dots, 10^4\}$ is trained via 5-fold cross validation, which is repeated 10 times to obtain standard deviations. This follows closely the setup in graph classification literature.

Table S5.: The set of hyperparameters that we use to train TOGL, along with their respective value ranges.

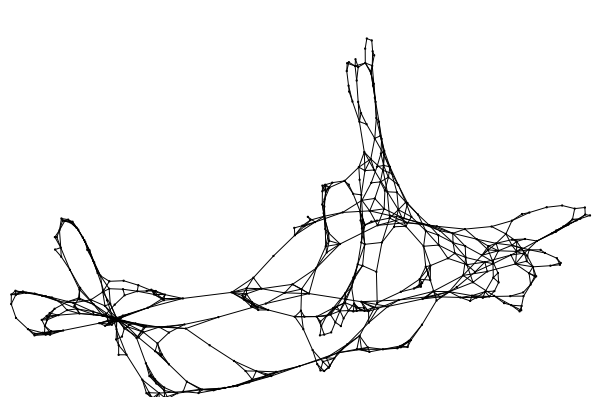
NAME	VALUE(S)
DeepSet	(True, False)
Depth	(3,4)
Dim1	(True)
Dropout	0.
Early Topo	(True, False)
Fake Topo	(True, False)
Filtration Hidden	32
Hidden Dimension	138–146
Num coordinate functions	3
Num filtrations	8
Residual and Batch Norm	(True)
Share filtration parameters	(True)

E. Visualization of the learnt filtrations

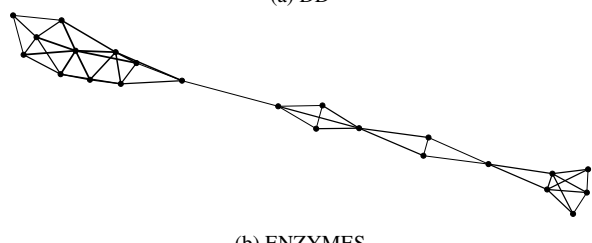
TOGL learns an arbitrary number of filtrations on the graphs. In Figure S8, we display 3 different filtrations learnt on a randomly picked graph from the DD dataset and compare it against the classical node degree filtration. The width of the nodes is plotted proportional to the node degree filtration while the color saturation is proportional to the learnt filtration. If Filtration 0 appears to be correlated with the degree filtration, other filtrations learnt by TOGL seem to focus on different local properties of the graph.

Table S6.: Test accuracy for the structure-based data sets PROTEINS-STRUCT, ENZYME-STRUCT, DD-STRUCT and MNIST-STRUCT.

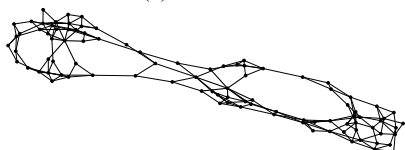
PROTEINS-STRUCT					
Depth	GCN	TopoGNN	TopoGNN (Interaction)	TopoGNN (Static)	TopoGNN (Static-Interaction)
1	68.6 ± 4.1	74.8 ± 4.0	75.3 ± 3.6	70.3 ± 3.9	71.0 ± 3.6
2	69.6 ± 3.1	74.6 ± 3.8	74.8 ± 3.2	70.7 ± 4.1	71.2 ± 4.7
3	70.6 ± 3.7	74.3 ± 3.5	74.3 ± 4.4	70.6 ± 3.7	70.0 ± 3.1
4	68.8 ± 2.8	74.6 ± 4.0	74.1 ± 2.5	70.7 ± 5.8	70.6 ± 3.1
5	67.7 ± 3.1	74.6 ± 3.6	74.6 ± 2.8	71.1 ± 1.7	71.1 ± 3.7
ENZYME-STRUCT					
Depth	GCN	TopoGNN	TopoGNN (Interaction)	TopoGNN (Static)	TopoGNN (Static-Interaction)
1	21.7 ± 5.3	26.0 ± 6.6	26.2 ± 6.9	24.8 ± 6.0	21.8 ± 4.0
2	23.5 ± 3.3	27.2 ± 6.4	23.0 ± 8.3	20.8 ± 4.0	21.5 ± 5.9
3	23.8 ± 3.9	27.3 ± 6.1	29.3 ± 7.9	24.5 ± 6.0	21.2 ± 3.4
4	22.0 ± 3.3	30.0 ± 7.0	29.8 ± 6.4	23.2 ± 5.7	22.7 ± 4.2
5	25.3 ± 5.6	29.5 ± 5.2	28.0 ± 6.2	25.8 ± 6.7	26.8 ± 5.3
DD-STRUCT					
Depth	GCN	TopoGNN	TopoGNN (Interaction)	TopoGNN (Static)	TopoGNN (Static-Interaction)
1	71.9 ± 5.1	75.5 ± 3.0	75.6 ± 2.9	69.4 ± 4.2	66.7 ± 3.2
2	71.1 ± 5.2	75.0 ± 2.3	75.9 ± 2.4	67.1 ± 3.3	66.5 ± 3.2
3	71.3 ± 5.1	75.0 ± 2.1	75.6 ± 2.2	68.8 ± 4.5	65.6 ± 2.2
4	70.8 ± 5.6	75.6 ± 2.5	74.9 ± 2.3	68.4 ± 2.6	64.4 ± 4.8
5	71.8 ± 5.1	76.1 ± 3.3	75.0 ± 2.4	67.7 ± 4.2	68.3 ± 3.6
MNIST-STRUCT					
Depth	GCN	TopoGNN	TopoGNN (Interaction)	TopoGNN (Static)	TopoGNN (Static-Interaction)
1	42.0 ± 2.2	62.6 ± 1.1	65.9 ± 0.4	60.0 ± 0.3	56.4 ± 0.4
2	56.4 ± 0.9	70.3 ± 2.4	77.1 ± 0.4	75.5 ± 0.2	70.5 ± 0.9
3	71.4 ± 0.9	77.9 ± 0.6	82.0 ± 0.3	81.7 ± 0.3	78.8 ± 0.8
4	76.2 ± 0.5	81.0 ± 0.4	84.3 ± 0.7	83.4 ± 0.4	82.0 ± 0.9
5	77.6 ± 0.4	81.3 ± 0.9	84.2 ± 0.3	85.1 ± 0.4	83.1 ± 0.5



(a) DD

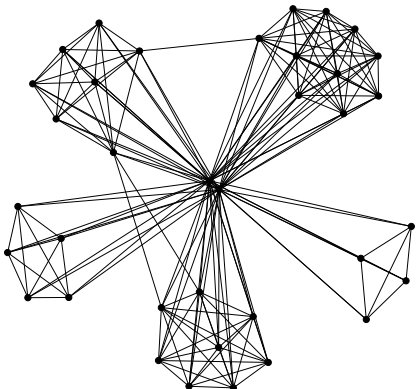


(b) ENZYMES

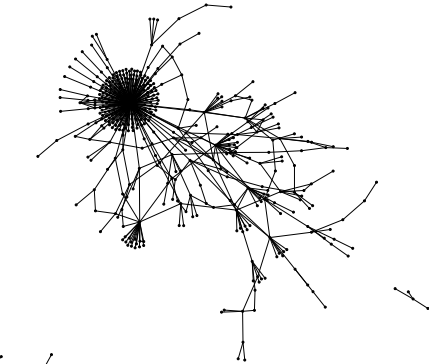


(c) PROTEINS

Figure S5.: Example graphs of the benchmark data sets that describe molecular structures. These graphs give rise to complex topological structures that can be exploited.

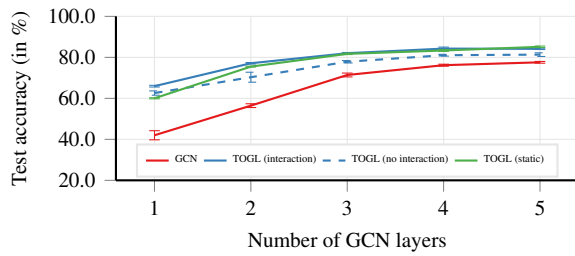


(a) IMDB-BINARY



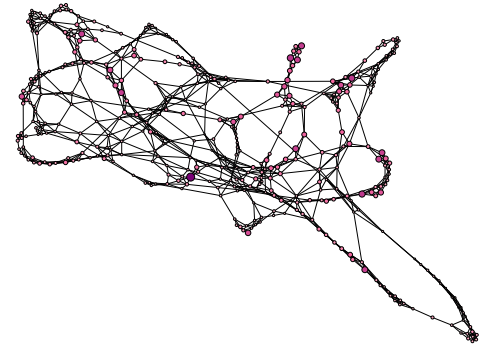
(b) REDDIT-BINARY

Figure S6.: Example graphs of the benchmark data sets that correspond to extracted social networks. These graphs are best described in terms of clique connectivity; the existence of a single ‘hub’ node does not give rise to a complex topological structure.

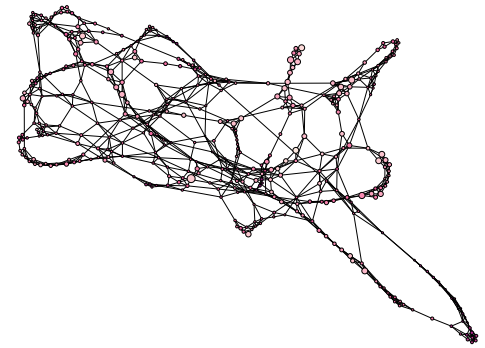


(a) Performance for MNIST-STRUCT

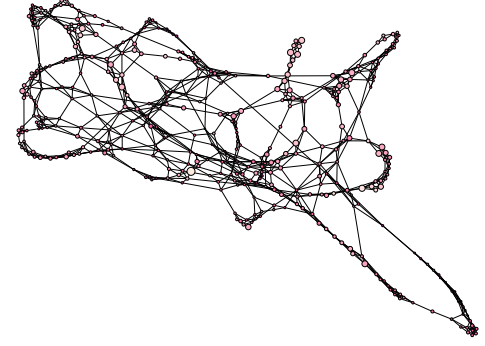
Figure S7.: Comparison of test accuracy for structure-based variants of the benchmark data sets while varying network depth. In contrast to the other data sets MNIST-STRUCT still contains information about the superpixel values but *no information about the positions* of the superpixels. This is due to the fact that MNIST has a relatively fixed connectivity structure, such that the classification task would be nearly impossible when discarding the pixel values.



(a) Filtration 0



(b) Filtration 1



(c) Filtration 2

Figure S8.: Examples of different filtrations jointly learnt on an example graph randomly picked from the DD dataset. The width of each node dot is proportional to its node degree, the colour saturation is proportional to the filtration value.